

Evidence for precession due to supercritical accretion in ultraluminous X-ray sources

Shan-Shan Weng¹, Hua Feng²

ABSTRACT

Most ultraluminous X-ray sources (ULXs) are thought to be supercritical accreting compact objects, where massive outflows are inevitable. Using the long-term monitoring data with the *Swift* X-ray Telescope, we identified a common feature in bright, hard ULXs: they display a quasi-periodic modulation in their hard X-ray band but not in their soft band. As a result, some sources show a bimodal distribution on the hardness intensity map. We argue that these model-independent results can be well interpreted in a picture that involves supercritical accretion with precession, where the hard X-ray emission from the central funnel is more or less beamed, while the soft X-rays may arise from the photosphere of the massive outflow and be nearly isotropic. It implies that precession may be ubiquitous in supercritical systems, such as the Galactic microquasar SS 433. How the hard X-rays are modulated can be used to constrain the angular distribution of the hard X-ray emission and the geometry of the accretion flow. We also find that two ULX pulsars (NGC 5907 ULX-1 and NGC 7793 P13) show similar behaviors but no bimodal distribution, which may imply that they have a different beaming shape or mechanism.

Subject headings: accretion, accretion disks — black hole physics — X-rays: binaries — X-rays: stars

1. Introduction

Ultraluminous X-ray sources (ULXs) are non-nuclear X-ray objects found in nearby galaxies (for reviews, see [Feng & Soria 2011](#); [Kaaret et al. 2017](#)). Their apparent luminosities exceed the Eddington limit of a $20 M_{\odot}$ black hole, or 3×10^{39} erg s⁻¹, suggesting that they may contain black holes more massive than those found in Galactic X-ray binaries ([Colbert & Mushotzky 1999](#)). However, the majority of ULXs may be super-Eddington accreting objects, resting on several observational evidence. First, three ULXs were identified to contain a neutron star accretor via the detection of coherent pulsations, while their apparent luminosities are well above the Eddington limit of a neutron star ([Bachetti et al. 2014](#); [Fürst et al. 2016](#); [Israel et al. 2017a,b](#)). Sec-

ond, on the perspective of X-ray spectra and spectral evolution, most ULXs do not behave in a manner similar to Galactic X-ray binaries at their sub-Eddington states ([Feng & Kaaret 2009](#); [Gladstone et al. 2009](#); [Kajava & Poutanen 2009](#); [Bachetti et al. 2013](#); [Sutton et al. 2013](#); [Middleton et al. 2014](#); [Walton et al. 2014](#)). Plus, direct evidence for fast outflows ([Pinto et al. 2016](#); [Walton et al. 2016b](#)), along with the fact that some of the surrounding nebulae are due to energetic outflows interacting with the environment ([Pakull & Mirioni 2003](#)), argues in favor of the supercritical accretion scenario ([Poutanen et al. 2007](#); [Ohsuga & Mineshige 2011](#); [Jiang et al. 2014](#); [Sądowski & Narayan 2016](#)). Thus, ULXs offer good opportunities for studying the accretion physics at extreme conditions.

As the accretion rate exceeds the Eddington limit, an analytical solution for the accretion flow becomes increasingly difficult ([Abramowicz et al. 1978, 1988](#); [Begelman 2002](#); [Gu et al. 2016](#)), but analytical analysis indicates that the disk must be inflated and powerful winds will be launched

¹Department of Physics and Institute of Theoretical Physics, Nanjing Normal University, Nanjing 210023, China

²Department of Engineering Physics and Center for Astrophysics, Tsinghua University, Beijing 100084, China

due to radiation pressure (Shakura & Sunyaev 1973; King & Pounds 2003; Poutanen et al. 2007; Shen et al. 2015). Numerical simulations generally confirm the presence of massive outflows despite inconsistent details between different groups (e.g., Ohsuga & Mineshige 2011; Jiang et al. 2014; Narayan et al. 2017).

Such a strong radiation pressure and outflow may have the natural consequence that it may have a significant impact back on the accretion disk and lead to precession. A remarkable example is the Galactic microquasar SS 433, which, though not a ULX, though, undergoes an extremely high accretion rate ($\sim 10^3$ times the Eddington limit) and shows strong outflows and obvious jet precession (Fabrika 2004). A possible analog of ULX may be M81 ULS-1, whose jet displayed a varying line-of-sight speed, and precession is a likely explanation (Liu et al. 2015).

As most ULXs do not show jets with atomic lines allowing for precession measurement, we thereby try to detect the signature of precession via its impact on the flux and spectral modulation. So far, *Swift* has monitored about a dozen of the ULXs covering a timescale of up to several years, leaving behind a legacy needed for such searches. In this paper, we collected monitoring data for nine ULXs with the X-ray Telescope (XRT) on *Swift*. The data analysis and results are presented in Section 2, and the physical implications are discussed in Section 3. We will show that, via a model-independent analysis, disk precession may be ubiquitous in ULXs.

2. Data and results

The *Swift* satellite has been scheduled to monitor bright ULXs, accumulated with thousands of observations. Most of these monitoring programs are dedicated for the study of long-term variability of ULXs including the search of periodic or quasi-periodic signals (e.g., Kaaret & Feng 2009; Strohmayer 2009; Grisé et al. 2013; Lin et al. 2015; Walton et al. 2016a; Hu et al. 2017). For a single observation, the typical exposure time is 1–3 ks, and the typical recurrent time between observations is 2–6 days. We collected ULXs that have been observed with *Swift* for at least 200 times as of 2017 August, but excluded those in M82 because they cannot be spatially resolved with XRT.

We also included the two known ULX pulsars for comparison, although the number of observations for them is much smaller and does not meet the above criterion. We end up with a sample of nine ULXs, including two accreting pulsars, NGC 5907 ULX-1 and NGC 7793 P13, and an intermediate-mass black hole (IMBH) candidate, ESO 243-49 HLX-1.

All of the observations of our interest were implemented in the photon-counting mode. We reduced the data using HEASOFT version 6.21. New event files were generated using the task *xrt-pipeline* with standard quality cuts. The script *xrtlccorr* was used to correct the effects caused by telescope vignetting and the point spread function. The source events were extracted from a circular region with a radius of 15 pixels centered at the source position, while the background contribution in the source aperture was estimated from a source-free region with a radius of 30 pixels. For each individual observation, we calculated its time-averaged net count rate, as one data point for further analysis. We further discarded data, where the 0.3–10 keV signal-to-noise ratio is no more than 2σ .

We calculated the Lomb–Scargle periodogram (Horne & Baliunas 1986) for ULXs to search for possible periodic or quasi-periodic signals. As the periodogram depends on the sampling, we only chose the part of the light curve that has a relatively high sampling rate and discarded a small fraction of data points largely separated in time, inclusion of which may cause an aliasing effect but will not affect the main conclusion. The fraction of observations in use is 633/649 for Holmberg (Ho) IX X-1, 572/585 for M81 X-6, 345/381 for NGC 1313 X-1, 342/378 for NGC 1313 X-2, 202/234 for NGC 4395 X-2, 371/479 for NGC 5408 X-1, 121/165 for NGC 5907 ULX-1, 82/112 for NGC 7793 P13, and 269/269 for ESO 243-49 HLX-1. The light curves are shown in Figure 1. The same data set was used for another analysis. We searched periodic signals in a timescale range from 10 days to one-half of the total time span of the selected time interval. The periodograms for both the hard band (1–10 keV) and the soft band (0.3–1 keV), are shown in Figure 2 for nine ULXs. The choice of 1 keV to separate the two bands because this is roughly the boundary between the soft and hard emission component in the X-ray

spectrum for most ULXs (Sutton et al. 2013; Middleton et al. 2015). A 4σ detection limit above the white noise is shown. We did not calculate the significance due to the presence of red noise, mainly because the relative strength of the modulation between the soft and hard energy bands, rather than the absolute significance, matters for the conclusion. In particular, the modulation due to precession may be unstable and will naturally produce a less significant periodic signal with respect to a strictly coherent signal. Plus, most of the data have been analyzed to search for periodic signals in the literature, where the significance has been carefully discussed.

The highest power for the hard band was found and marked in the plot; if several significant peaks or possible harmonics are shown, the one with the shortest period is chosen, because it is supported by more cycles. Then the corresponding peak in the soft band is identified for comparison. The light curves folded at the most likely period are shown in Figure 3 for the two bands. We emphasize that the second rule only applies to Ho IX X-1 and M81 X-6, for which no matter which peak is selected, the conclusion remains: stronger modulation in the hard band than in the soft band.

The observed flux (count rate) distribution for each ULX in 1–10 keV is shown in Figure 4. Some sources show a bimodal distribution, while others do not. We fitted the flux distribution with Gaussians and the errors for small counts were treated using the statistic in Gehrels (1986, $1 + \sqrt{N} + 0.75$ for $N < 5$, or \sqrt{N} otherwise). F-test indicates that the second Gaussian component has a chance probability of 1×10^{-7} , 7×10^{-12} , 2×10^{-22} , respectively, for Ho IX X-1, M81 X-6, and NGC 1313 X-2. On the other hand, for the rest of ULXs, a single Gaussian can adequately fit the flux distribution. On each plot, the dashed green line marks the 2σ detection limit given a typical *Swift* exposure of 1 ks. This suggests that the lower-flux peak in the bimodal distribution is not an observational effect. The flux distributions in the 0.3–1 keV energy band is shown in Figure 5. None of the ULXs shows a bimodal distribution in the soft band.

In Figure 6, we plotted the ratio of count rates between the hard and soft bands (1–10 keV/0.3–1 keV) versus the observed XRT count rate in 0.3–10 keV, *a.k.a.* the hardness intensity diagram (HID). As one can see, the bimodal distribution is even

more obvious on the two-dimensional plane; the same three ULXs show two islands of points on the HID, corresponding to a low/soft and a high/hard regime, respectively. NGC 1313 X-1 also shows a possible bimodal distribution, but not significant enough due to a small number of points in the high/hard regime. We emphasize that both the intensity and the hardness are direct observables with *Swift* XRT. If absorption corrected quantities are used, the two peaks will be more distinct.

We summarize the above results in Table 1, including whether or not they show a bimodal distribution on the HID, the luminosity ratio of the two peaks for the bimodal feature, the significance of the power in the soft and hard bands (*moderate* means close to or slightly above 4σ , otherwise being *strong* or *weak*), the peak period if the hard X-ray periodicity is strong or moderate, and the power ratio at the peak between the hard and soft bands.

3. Discussion and conclusion

Some of the findings in this paper have been reported in the literature. For NGC 5408 X-1, no significant periodicity is found but the two peaks (near 110 days and 190 days) shown in Figure 2 are consistent with previous reports (Grisé et al. 2013; Pasham & Strohmayer 2013; Lin et al. 2015). Lin et al. (2015) detected a significant quasi-periodic signal around ~ 625 days for Ho IX X-1; we detected this peak but considered the one at 266 days as the tentative peak, as there are only four cycles to support the longer period. They also found that the periodicity was not stable for M81 X-6, varying from ~ 370 days in an earlier segment to ~ 110 days later, which was adopted by this work. For HLX-1, the detected period was actually due to recurrent outbursts (Yan et al. 2015), which have been found evidently delayed in recent cycles, see Figure 1. Therefore, although a strong peak in the periodogram in the soft band is detected, we do not consider it to be a quasi-periodic signal. Luangtip et al. (2016) fitted the XRT spectra of Ho IX X-1 with a power-law model and found that the ULX exhibited a similar bimodal distribution on the power-law photon index versus the flux plane, consistent with our results. They also attribute the degeneracy between the spectral shape and luminosity as due to source precession. Here,

TABLE 1
SUMMARY OF THE PROPERTIES OF ULXS IN THE SAMPLE.

Source	Bimodal on HID (Flux Ratio [†])	Periodicity		
		1–10 keV	0.3–1 keV	Power Ratio
Ho IX X-1	yes (2.2)	strong (266 days)	moderate	52.8/26.9 = 1.9
M81 X-6	yes (2.3)	strong (115 days)	weak	31.7/6.2 = 5.1
NGC 1313 X-1	likely	moderate (212 days)	weak	17.2/13.7 = 1.3
NGC 1313 X-2	yes (3.2)	strong (158 days)	weak	30.5/10.4 = 2.9
NGC 4395 X-2	no	weak	weak	12.0/13.2 = 0.9
NGC 5408 X-1	no	weak	weak	10.9/5.0 = 2.2
NGC 5907 ULX-1	no	strong (79 days)	weak	29.2/3.4 = 8.7
ESO 243-49 HLX-1	no	moderate (184 days)	strong	16.3/28.7 = 0.6

[†]The flux ratio is quoted as the ratio of the count rate for the two peaks in 1-10 keV (Figure 4, and the typical statistical error is 0.1.

we combine both the temporal and spectral behaviors of these sources to confine the nature of ULXs.

The results clearly classify the ULXs into two categories. Four ULXs (Ho IX X-1, M81 X-6, NGC 1313 X-1, and X-2) exhibit a strong (or moderate for NGC 1313 X-1) modulation in the hard band, however, at the same period, the modulation in the soft band is much weaker or absent. The sources showing such a feature also display a bimodal distribution on the HID; a similar bimodal feature can also be reflected on the flux distribution. Two ULXs (NGC 4395 X-2 and NGC 5408 X-1) do not show a significant modulation, nor do they have a bimodal distribution on the HID. These two sources are the softest among all, see the HID in Figure 6 (we note that they are indeed the softest after correction for absorption). For such soft ULXs, whether or not a cut at 1 keV can separate the two emission components is a question; a cut at higher energies will lead to less photons in the hard band and difficulties in detection.

We argue that these results can be well explained as due to supercritical accretion with precession. As mentioned in the Introduction, most ULXs are thought to be systems undergoing supercritical accretion. A supercritical accretion flow around a stellar mass black hole may produce

two emitting components, a soft, quasi-blackbody component with a temperature of several tenths of a keV arising from the photosphere of the outflow that covers the outer disk, and a hard, Comptonized component from the inner accretion disk (below the inner photospheric radius, see Poutanen et al. 2007). Such a picture has been generally confirmed by recent numerical simulations (Ohsuga & Mineshige 2011; Jiang et al. 2014; Sądowski & Narayan 2016), and can be used to explain the spectral-timing behaviors of bright ULXs (Middleton et al. 2015). As the emission from the inner disk can only be seen via a central funnel enclosed by the thick outflow, the hard X-rays could be collimated, while the soft X-rays are almost isotropic. In this picture, precession of the accretion flow will cause a larger modulation factor on the hard X-ray flux than on the soft X-ray flux. Whether or not there is a bimodal distribution of the hard X-ray flux depends on its angular distribution. For instance, in an extreme condition where the hard X-rays are strictly collimated by the wall of the central cone, a bimodal distribution is naturally seen when the hard X-ray beam enters and leaves the line of sight. In practice, the hard X-ray emission may have an angular distribution much wider than the open angle of the funnel, due to multiple scattering below the scattering photosphere (Jiang et al. 2014). Thus, the folded light curve may be useful to model the hard X-ray angu-

lar distribution, or the geometry of the accretion flow. Upon the assumptions above, our results suggest that the hard X-ray emission is more or less beamed and very likely originated from the central funnel.

The two pulsars NGC 5907 ULX-1 and NGC 7793 P13, like other ULXs, display strong modulation in the hard X-ray band but not in the soft band. However, it does not show a bimodal distribution on the HID. As discussed above, the bimodal distribution depends on how the hard X-ray emission is modulated. The folded light curve of the pulsar displays a smooth transition from the peak to valley like a triangle waveform. This may imply that the pulsar has a different shape or mechanism of beaming, indicating that other ULXs may contain a black hole instead of a neutron star. We want to emphasize that this preliminary conclusion is based on only two sources, and the number of observations for these two pulsars are small compared with other ULXs. So, along with the fact that ESO 243-49 HLX-1 does not show a bimodal feature, the conclusion is tentative and should be further tested with more observations.

The hyperluminous X-ray source ESO 243-49 HLX-1 has been argued to be a good candidate for an IMBH (Farrell et al. 2009). It shows possible periodicity, stronger in the soft band than in the hard band, that is obviously due to recurrent outbursts (Yan et al. 2015), which have evidently been found to have been delayed in recent cycles. This clearly distinguishes this source from other ULXs.

To conclude, a hard X-ray quasi-periodicity along with a nearly constant soft X-ray flux is quite consistent with the scenario described above that the sources are undergoing supercritical accretion with precession. The absence of such features seems to belong to the softest ULXs, which are argued to be more inclined systems (Sutton et al. 2013; Middleton et al. 2015), where the precession angle may be smaller than the inclination angle, even if the precession occurs. The results suggest that precession may be ubiquitous in supercritical accretion systems like SS 433, as a natural consequence of strong radiation pressure and outflows.

We thank the anonymous referee for useful com-

ments, and Junxian Wang and Zhenyi Cai for helpful discussions. This work is supported by the National Natural Science Foundation of China under grants 11673013, 11573023, and 11633003, and the National Program on Key Research and Development Project (Grant No. 2016YFA040080X).

REFERENCES

- Abramowicz, M., Jaroszynski, M., & Sikora, M. 1978, *A&A*, 63, 221
- Abramowicz, M. A., Czerny, B., Lasota, J. P., & Szuszkiewicz, E. 1988, *ApJ*, 332, 646
- Bachetti, M., Rana, V., Walton, D. J., et al. 2013, *ApJ*, 778, 163
- Bachetti, M., Harrison, F. A., Walton, D. J., et al. 2014, *Nature*, 514, 202
- Begelman, M. C. 2002, *ApJ*, 568, L97
- Colbert, E. J. M., & Mushotzky, R. F. 1999, *ApJ*, 519, 89
- Fabrika, S. 2004, *Astrophysics and Space Physics Reviews*, 12, 1
- Farrell, S. A., Webb, N. A., Barret, D., Godet, O., & Rodrigues, J. M. 2009, *Nature*, 460, 73
- Feng, H., & Kaaret, P. 2009, *ApJ*, 696, 1712
- Feng, H., & Soria, R. 2011, *New A Rev.*, 55, 166
- Fürst, F., Walton, D. J., Harrison, F. A., et al. 2016, *ApJ*, 831, L14
- Gehrels, N. 1986, *ApJ*, 303, 336
- Gladstone, J. C., Roberts, T. P., & Done, C. 2009, *MNRAS*, 397, 1836
- Grisé, F., Kaaret, P., Corbel, S., Cseh, D., & Feng, H. 2013, *MNRAS*, 433, 1023
- Gu, W.-M., Sun, M.-Y., Lu, Y.-J., Yuan, F., & Liu, J.-F. 2016, *ApJ*, 818, L4
- Horne, J. H., & Baliunas, S. L. 1986, *ApJ*, 302, 757
- Hu, C.-P., Li, K. L., Kong, A. K. H., Ng, C.-Y., & Lin, L. C.-C. 2017, *ApJ*, 835, L9

- Israel, G. L., Belfiore, A., Stella, L., et al. 2017a, *Science*, 355, 817
- Israel, G. L., Papitto, A., Esposito, P., et al. 2017b, *MNRAS*, 466, L48
- Jiang, Y.-F., Stone, J. M., & Davis, S. W. 2014, *ApJ*, 796, 106
- Kaaret, P., & Feng, H. 2009, *ApJ*, 702, 1679
- Kaaret, P., Feng, H., & Roberts, T. P. 2017, *ARA&A*, 55, 303
- Kajava, J. J. E., & Poutanen, J. 2009, *MNRAS*, 398, 1450
- King, A. R., & Pounds, K. A. 2003, *MNRAS*, 345, 657
- Lin, L. C.-C., Hu, C.-P., Kong, A. K. H., et al. 2015, *MNRAS*, 454, 1644
- Liu, J.-F., Bai, Y., Wang, S., et al. 2015, *Nature*, 528, 108
- Luangtip, W., Roberts, T. P., & Done, C. 2016, *MNRAS*, 460, 4417
- Middleton, M. J., Heil, L., Pintore, F., Walton, D. J., & Roberts, T. P. 2015, *MNRAS*, 447, 3243
- Middleton, M. J., Walton, D. J., Roberts, T. P., & Heil, L. 2014, *MNRAS*, 438, L51
- Narayan, R., Sądowski, A., & Soria, R. 2017, *MNRAS*, 469, 2997
- Ohsuga, K., & Mineshige, S. 2011, *ApJ*, 736, 2
- Pakull, M. W., & Mirioni, L. 2003, in *Revista Mexicana de Astronomia y Astrofisica*, vol. 27, Vol. 15, *Revista Mexicana de Astronomia y Astrofisica Conference Series*, ed. J. Arthur & W. J. Henney, 197–199
- Pasham, D. R., & Strohmayer, T. E. 2013, *ApJ*, 771, 101
- Pinto, C., Middleton, M. J., & Fabian, A. C. 2016, *Nature*, 533, 64
- Poutanen, J., Lipunova, G., Fabrika, S., Butkevich, A. G., & Abolmasov, P. 2007, *MNRAS*, 377, 1187
- Sądowski, A., & Narayan, R. 2016, *MNRAS*, 456, 3929
- Shakura, N. I., & Sunyaev, R. A. 1973, *A&A*, 24, 337
- Shen, R.-F., Barniol Duran, R., Nakar, E., & Piran, T. 2015, *MNRAS*, 447, L60
- Strohmayer, T. E. 2009, *ApJ*, 706, L210
- Sutton, A. D., Roberts, T. P., Gladstone, J. C., et al. 2013, *MNRAS*, 434, 1702
- Walton, D. J., Harrison, F. A., Grefenstette, B. W., et al. 2014, *ApJ*, 793, 21
- Walton, D. J., Fürst, F., Bachetti, M., et al. 2016a, *ApJ*, 827, L13
- Walton, D. J., Middleton, M. J., Pinto, C., et al. 2016b, *ApJ*, 826, L26
- Yan, Z., Zhang, W., Soria, R., Altamirano, D., & Yu, W. 2015, *ApJ*, 811, 23

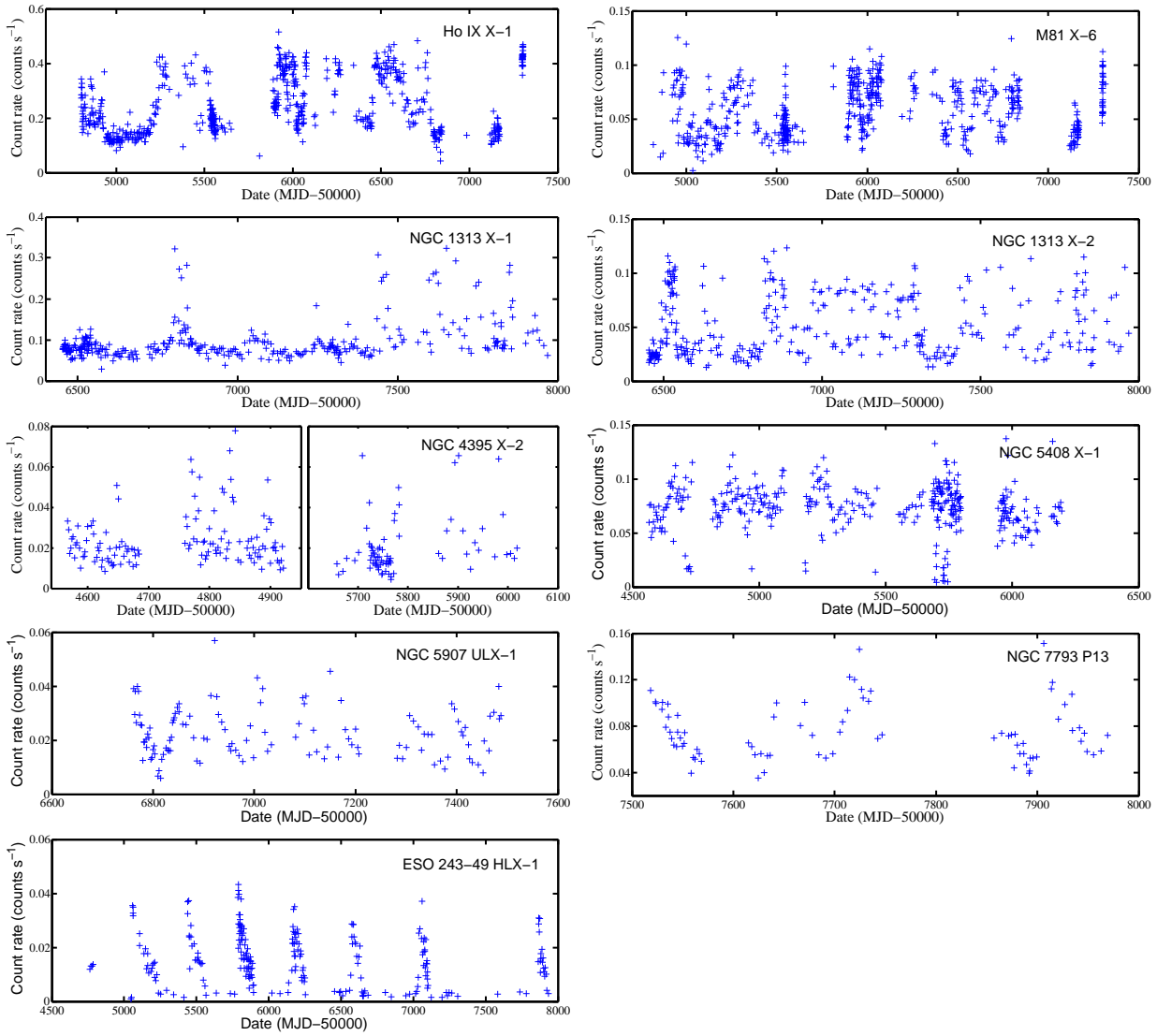


Fig. 1.— *Swift*/XRT 0.3–10 keV light curves (observed count rates) for ULXs in our sample. Due to uneven sampling, we only adopt the duration when the sampling is the densest for each source. A small fraction of data that are largely separated in time are discarded.

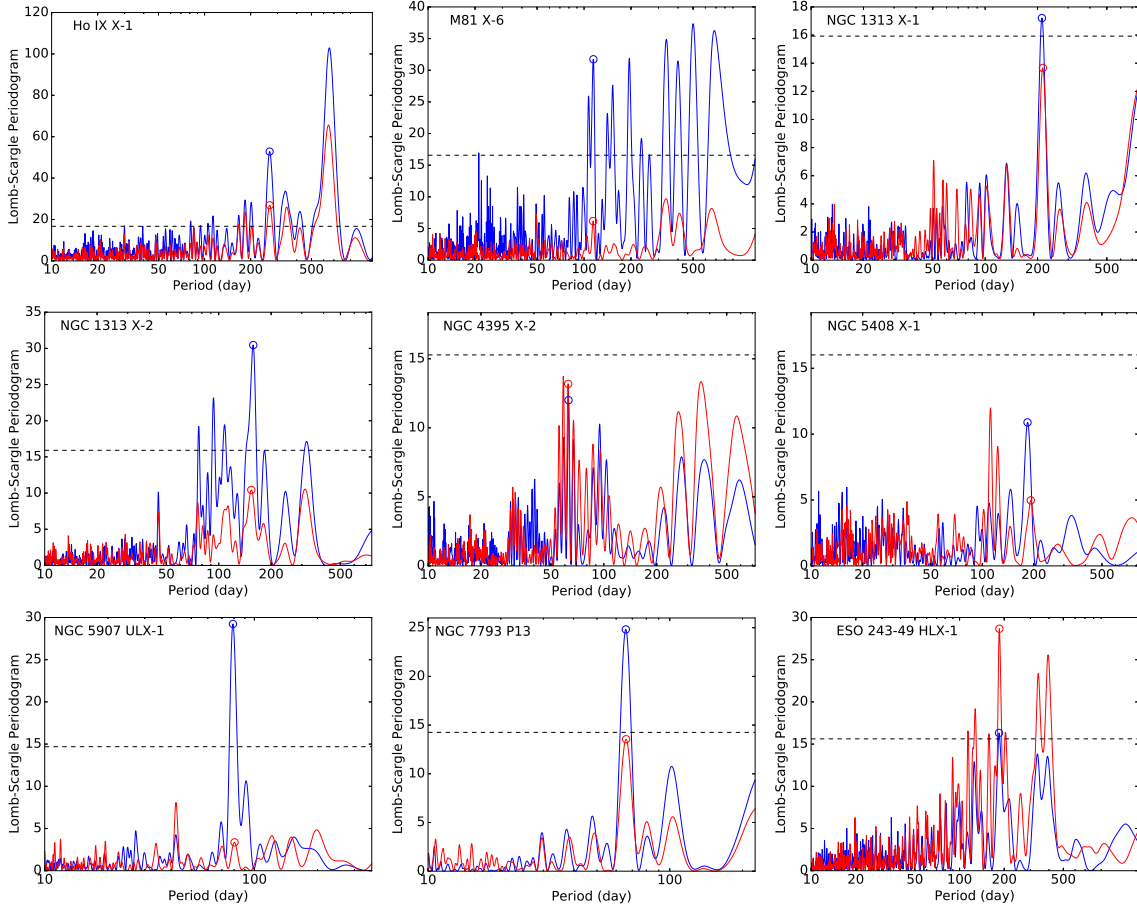


Fig. 2.— Lomb–Scargle periodograms for ULXs in the sample with high quality light curves. The dashed line indicates a 4σ detection above the white noise. The blue line is for the hard band (1–10 keV) and the red is for the soft band (0.3–1 keV). The blue circle indicates the peak of the power in the hard band; if there are possible harmonics or multiple significant peaks, the one of the shortest period is chosen. The red circle marks the corresponding peak in the soft band.

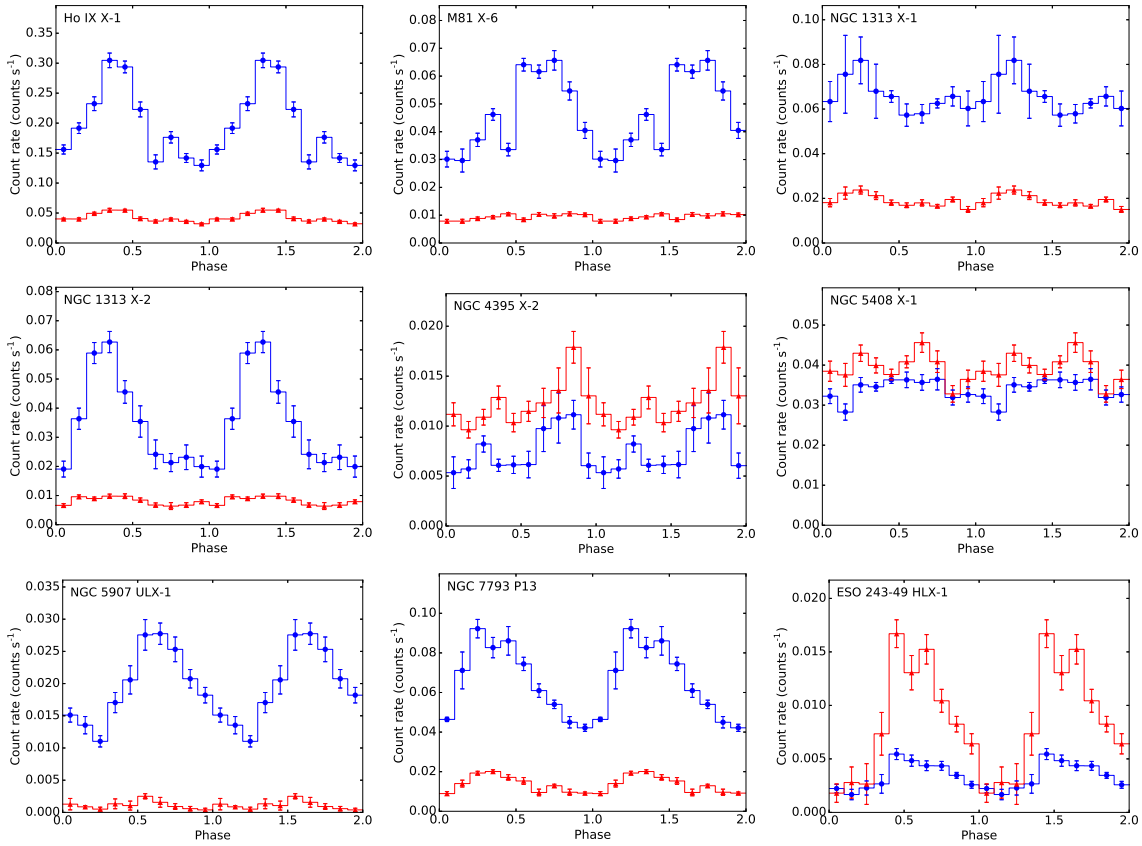


Fig. 3.— Light curves folded at their most likely period (indicated by the blue circle in Figure 2). The blue is for the hard band (1–10 keV) and the red is for the soft band (0.3–1 keV).

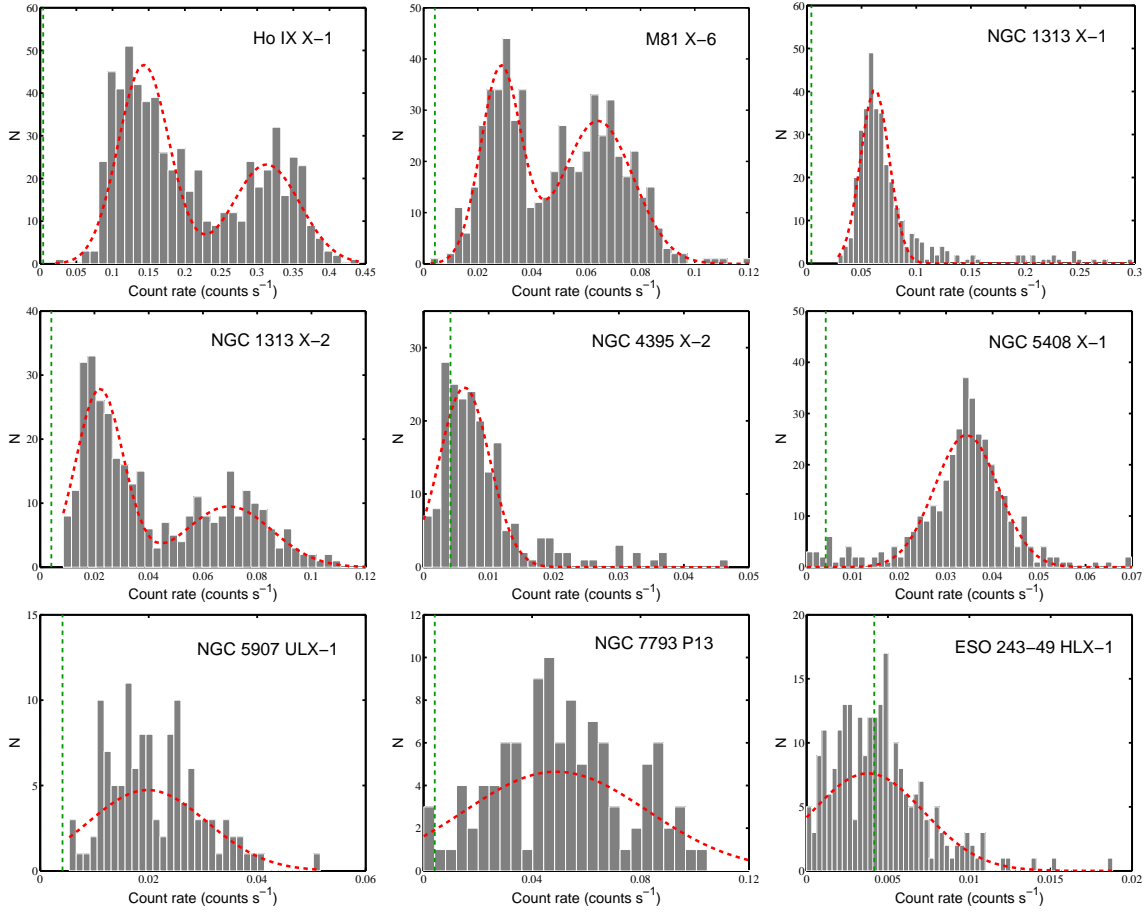


Fig. 4.— Distributions of the *Swift* XRT 1–10 keV count rate for ULXs in the sample. Each histogram is fitted by a Gaussian function or two if needed. The green dashed line marks the 2σ detection limit for a 1000 s observation.

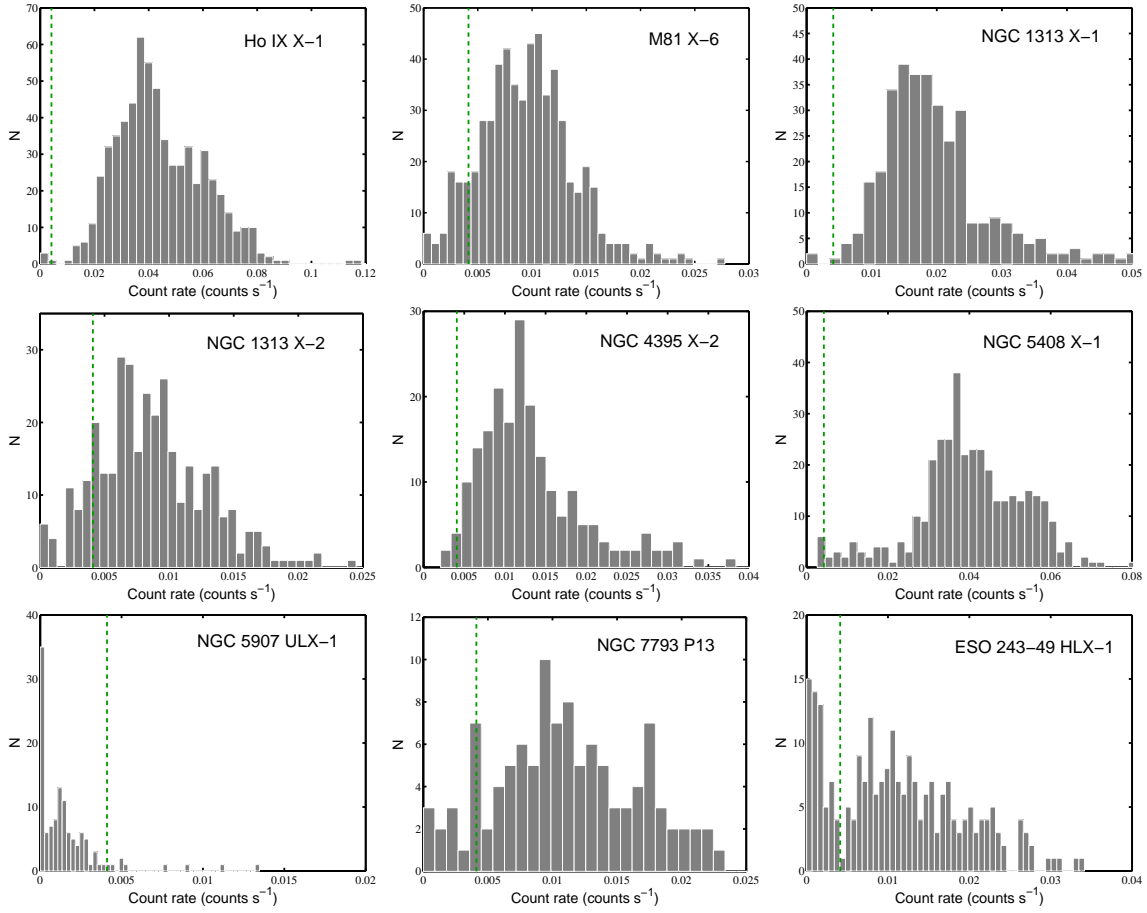


Fig. 5.— Same as Figure 4 but in the energy band of 0.3–1 keV.

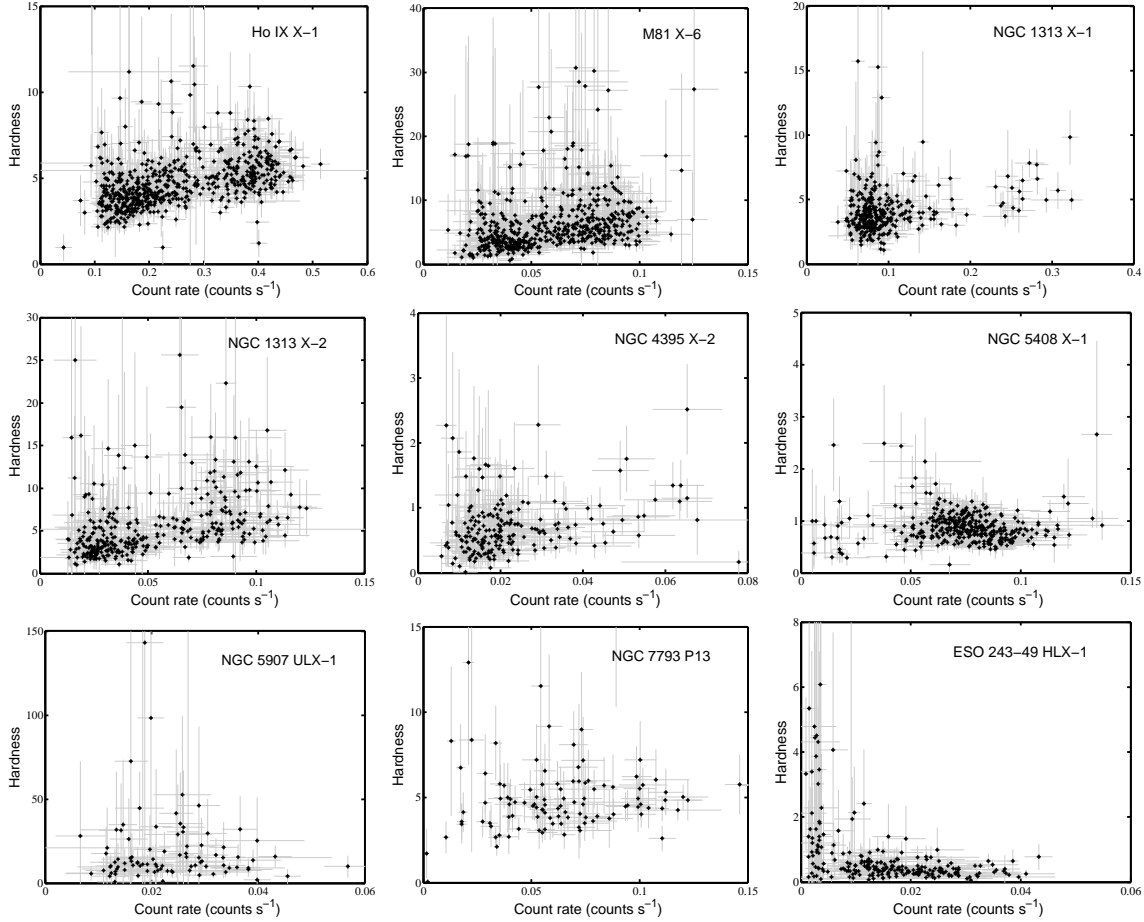


Fig. 6.— HIDs for ULXs in the sample. The hardness is defined as the ratio of XRT count rates between the hard band (1–10 keV) and the soft band (0.3–1 keV). The intensity refers to the 0.3–10 keV count rate measured with XRT. Each point represents a *Swift* observation and the errors are of 1σ .